http://www.jmaterenvironsci.com

JMES

Experimental and theoretical studies on inhibition of Quinoxaline derivatives against corrosion of mild steel in acidic medium

A. Zouitini[1], Y. Kandri Rodi[1], H. Elmsellem[2*], H. Steli[6], F. Ouazzani Chahdi[1], M. Ali Shariati[5], A. E. Janati[1], Y. Ouzidan[1], N. K. Sebbar[2], E. M. Essassi[3,4]

[1]Laboratory of Applied Organic Chemistry, Faculty of Science and Technology, University Sidi Mohammed Ben Abdallah, Fez, Morocco.
[2]Laboratoire de chimie analytique appliquée, matériaux et environnement (LC2AME), Faculté des Sciences, B.P. 717, 60000 Oujda, Morocco.
[3]Laboratoire de Chimie Organique Hétérocyclique, URAC 21, Pôle de Compétences Pharmacochimie, Mohammed V University in Rabat, Faculté des Sciences, Av. Ibn Battouta, BP 1014 Rabat, Morocco.
[4]Moroccan Foundation for Advanced Science, Innovation and Research (MASCIR), Rabat Design Center, Rue Mohamed Al Jazouli, Madinat El Irfane, Rabat, Morocco.
[5]Research Department, LLC «Science & Education», and Researcher, All Russian Research Institute of Phytopathology, Moscow Region, Russia.
[6]Laboratoire mécanique & énergétique, Faculté des Sciences, Université Mohammed Premier, Oujda, Morocco.

Abstract
The inhibitory effect of 1,4-diallyl-6-methylquinoxaline-2,3(1H,4H)-dione (2) on the corrosion of mild steel in 1 M hydrochloric acid was studied using mass loss, potentiodynamic polarization technique and electrochemical impedance spectroscopy measurements at 308K. The investigation results indicate that the Quinoxaline derivative with an average efficiency of 86% at 10-3M of additive concentration have fairly effective inhibiting properties for mild steel in hydrochloric acid, and acts as cathodic type inhibitor character. The inhibition efficiencies measured by all measurements show that the inhibition efficiencies increase with increase in inhibitor concentration. This reveals that the inhibitive mechanism of inhibitors was primarily due to adsorption on mild steel surface, and followed Langmuir adsorption isotherm. Moreover, to provide further insight into the mechanism of inhibition, quantum chemical calculations of the inhibitor were performed.

1. Introduction

Quinoxaline derivatives are an important class of heterocyclic compounds, in which N replaces one or more carbon atoms of the naphthalene ring [1]. They are important in industry due to their ability to inhibit the metal corrosion [2-5], in the preparation of the porphyrins, since their structure is similar to the chromophores in the natural system, and also in the electroluminescent materials [6]. In pharmacological industry, they have absorbed a great deal of attention due to their wide spectrum of biological properties [1, 7-10]. For example, they can be used against bacteria, fungi, virus, leishmania, tuberculosis, malaria, cancer, depression, and neurological activities, among others. The quinoxaline structural nucleus renders all these activities possible. Quinoxaline structure acts as a precursor to assembly a large number of new compounds for diverse applications [1]. Recent demonstrations showed that 1,4-diallyl-6-methylquinoxaline-2,3(1H,4H)-dione derivatives act a good inhibitor for the corrosion of mild steel in 1M HCl [11] **Figure 1**.

2. Experimental
2.1. Materials
In this study our material was the mild steel with a chemical composition (in wt %) of 0.09 % P; 0.38 % Si; 0.01 % Al; 0.05 % Mn; 0.21 % C; 0.05 % S and the remainder iron (Fe). Two batches of tests were performed, we report here on the average values.
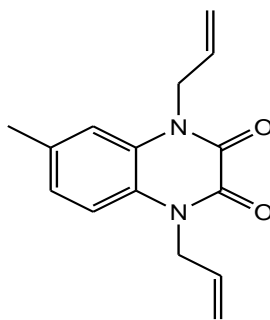
Figure 1 : Chemical structure of 1,4-diallyl-6-methylquinoxaline-2,3(1H,4H)-dione (**2**).

2.2. Synthesis of inhibitor
  ✓ *Synthesis of 6-methyl-1,4-dihydroquinoxaline-2,3-dione (**1**)*

To a solution of 4-methyl-o-phenylenediamine **1** (8 mmol) was added oxalic acid 2 (8 mmol) in 16 ml of hydrochloric acid (4M). The mixture was refluxed for 4 hours. The black precipitate obtained is washed several times with distilled water (Scheme1).

  ✓ *Synthesis of inhibitor* 1,4-diallyl-6-methylquinoxaline-2,3(1H,4H)-dione *(**2**).*

To a solution of 6-methyl-1,4-dihydroquinoxaline-2,3-dione 0,3g (1,73 mmol) in DMF (20 ml), were added 0.47g (3,61 mmol) of potassium carbonate and 0,1 mmol of tetra-n-butyl ammonium bromide (TBAB). After 10 minutes of stirring 3,46 mmol of allyl bromide was added, then the mixture was allowed to stir at room temperature for 12 hours. After filtration of salts, the solution was evaporated under reduced pressure and the residue obtained was dissolved in dichloromethane, the organic phase was dried over Na2SO4 and then concentrated. The mixture obtained was chromatographed on silica gel column (eluent: hexane/ethylacetate (3/1)) (Scheme1).

Scheme 1. Synthesis of 1,4-diallyl-6-methylquinoxaline-2,3(1H,4H)-dione (**2**).
The analytical and spectroscopic data are conforming to structures of compounds (**1**) and (**2**) formed. ^{1}H-NMR and ^{13}C-NMR spectrums of compound (**2**) are showed below (Figure 2).
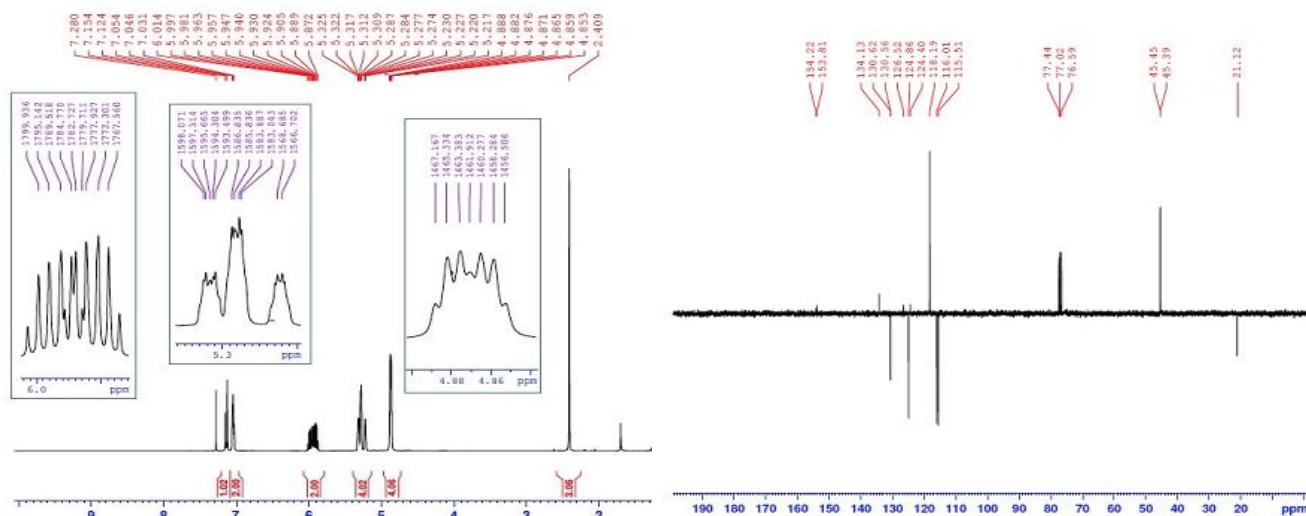

Figure 2: ^{1}H-NMR and ^{13}C-NMR spectrums of 1,4-diallyl-6-methylquinoxaline-2,3(1H,4H)-dione (**2**).

(1):Yield: 90**%; mp:** 536**K; RMN^{1}H (DMSO-d6) δ ppm:** 2,26 (s, 3H, C***H₃***) ; 6,87-7,28 (m, 3H, C***H***$_{arom}$) ; 11,83 (s, 2H, 2 N***H***);**RMN^{13}C (DMSO-d6) δ ppm**: 155,76 (***C***=O) ; 155,44 (***C***=O) ; 132,73 (***C***q) ; 125,92 (***C***q) ; 124,23 (***C***H$_{arom}$) ; 123,76 (***C***q) ; 115,61 (***C***H$_{arom}$) ; 115,44 (***C***H$_{arom}$) ; 21,01 (***C***H₃).

(2):Yield: 92**%; mp:** 306**K; RMN^{1}H (DMSO-d6) δ ppm:** 2,40 (s, 3H, C***H₃***) ; 4,87 (m, 4H, 2CH=C***H₂***) ; 5,31 (m, 4H, 2N-C***H₂***) ; 5,94 (m, 2H, 2C***H***=CH₂) ;7,03-7,15 (m, 3H, C***H***$_{arom}$) ; **RMN^{13}C (DMSO-d6) δ ppm**: 154,22 (***C***=O) ; 153,81 (***C***=O) ; 134,13 (***C***q) ; 130,56 (***C***H$_{arom}$) ;126,52 (***C***q) ; 124,85 (2***C***H$_{arom}$) ; 124,75 (***C***H$_{arom}$) ;124,40 (***C***q) ; 118,19 (2***C***H₂) ; 116,01 (***C***H=CH₂) ; 115,51 (***C***H=CH₂) ; 45,45 (N-***C***H₂) ;45,39 (N-***C***H₂) ; 28,90 (2***C***H₂) ; 21,12 (***C***H₃).

2.3. Materials and solutions

2.3.1. Weight loss measurement

the gravimetric study were performed using sheets in dimensions of 1.5cm x 1.5cm x 0.25cm, in order to prepare the specimens, the sheets were abraded by different grades of emery papers (180, 400, 800, 1000, 1200), and washed by bidistilled wated, degreased by acetone and dried. The experiments carried out in 1M HCl medium, triplicate experiences were made to ensure the reproducibility. The inhibition efficiency E_w% was calculated using the following equation:

$$EW(\%) = \frac{\text{Wcorr} - \text{Wcorr}/\text{inh}}{\text{Wcorr}} \times 100 \text{ Wcorr} \quad (1)$$

W_{corr} and $_{Wcorr/inh}$ are the corrosion rate of steel without and with inhibitors, respectively.

2.3.2. Electrochemical measurements

Electrochemical experiments were recorder using a potentiostat PGZ 100 piloted by Voltamaster software, the electrochemical measurements were carried out in conventional three electrode electrolysis cylindrical Pyrex glass cell. The working electrode (WE) has the form of a disc cut from the steel sheet, the area that is exposed to the corrosive solution was 1 cm^2.A satured calomel electrode (SCE) and a platinum electrode were used respectively as reference and auxiliary electrode. The temperature of the cell was controlled by a thermostatically at 308 K. Before start any test, it is necessary that the potential must stabilized for 30 min. The electrochemical impedance spectroscopy (EIS) measurements are carried out with the electrochemical system, which included a digital potentiostat model Voltalab PGZ100 computer at E$_{corr}$ after immersion in solution without bubbling. After the determination of steady-state current at a corrosion potential, sine wave voltage (10 mV) peak to peak, at frequencies between 100 kHz and 10 mHz are superimposed on the rest potential. Computer programs automatically controlled the measurements performed at rest potentials after 0.5 hour of exposure at 308 K. The impedance diagrams are given in the Nyquist representation. Each experiment was repeated at least three times to check the reproducibility.

The inhibition efficiency was calculated from the charge transfer resistance values using the following equation:

$$E\% = ((R_{ct} - R^0_{ct}) / R_{ct}) \text{ x100} \quad (2)$$

R_{ct} and R^0_{ct} are the charge transfer resistance in absence and in presence of inhibitor, respectively.

The polarisation curves are obtained from −800 mV to −200 mV with a scan rate equal 1mV per second vs. free corrosion potential (E_{corr} vs. SCE). The inhibition efficiency was evaluated from the measured I_{corr} values using the following relationship:

$$EI(\%) = \frac{I\text{corr} - I\text{corr(i)}}{I\text{corr}} \text{x100} \quad (3)$$

Where I_{corr} and $I_{corr(i)}$ are the corrosion current densities for steel electrode in the uninhibited and inhibited solutions, respectively.

2.3. Theory and computational details

Quantum chemical calculations are used to correlate experimental data for inhibitors obtained from different techniques (viz., electrochemical and weight loss) and their structural and electronic properties. According to Koop man's theorem [12], E$_{HOMO}$ and E$_{LUMO}$ of the inhibitor molecule are related to the ionization potential (I) and the electron affinity (A), respectively. The ionization potential and the electron affinity are defined as I = −E$_{HOMO}$ and A = −E$_{LUMO}$, respectively. Then absolute electronegativity (χ) and global hardness (η) of the inhibitor molecule are approximated as follows [13]:

$$\chi = \frac{I+A}{2} \ , \ \chi = -\frac{1}{2}(E_{HOMO} - E_{LUMO}) \quad (4)$$

$$\eta = \frac{I-A}{2} \ , \ \eta = -\frac{1}{2}(E_{HOMO} - E_{LUMO}) \quad \textbf{(5)}$$

Where I = -E_{HOMO} and A= -E_{LUMO} are the ionization potential and electron affinity respectively.

The fraction of transferred electrons ΔN was calculated according to Pearson theory [12]. This parameter evaluates the electronic flow in a reaction of two systems with different electronegativities, in particular case; a metallic surface (Fe) and an inhibitor molecule. ΔN is given as follows:

$$\Delta N = \frac{\chi_{Fe} - \chi_{inh}}{2(\eta_{Fe} + \eta_{inh})} \quad \textbf{(6)}$$

Where χ_{Fe} and χ_{inh} denote the absolute electronegativity of an iron atom (Fe) and the inhibitor molecule, respectively; η_{Fe} and ηinh denote the absolute hardness ofFe atom and the inhibitor molecule, respectively. In order to apply the eq.6 in the present study, a theoretical value for the electronegativity of bulk iron was used χ_{Fe} = 7 eV and a global hardness of η_{Fe} = 0, by assuming that for a metallic bulk I = A because they are softer than the neutral metallic atoms [14]. The electrophilicity has been introduced by Sastri and al. [13], is a descriptor of reactivity that allows a quantitative classification of the global electrophilic nature of a compound within a relative scale. They have proposed the ω as a measure of energy lowering owing to maximal electron flow between donor and acceptor and ω is defined as follows.

$$\omega = \frac{\chi^2}{2\eta} \quad \textbf{(7)}$$

The Softness σ is defined as the inverse of the η [15]

$$\sigma = \frac{1}{\eta} \quad \textbf{(8)}$$

3. Results and discussion

3.1. Weight loss measurement

Table 1 shows the weight loss measurement results and inhibition efficiencies for varying concentrations of inhibitor 1,4-diallyl-6-methylquinoxaline-2,3(1H,4H)-dione (**2**) in HCl 1M at 308 K. The amount of weight loss is seen to decrease with increasing additive concentration for each compound. Instead, the highest inhibition efficiencies is observed for 1,4-diallyl-6-methylquinoxaline-2,3(1H,4H)-dione (**2**) and reach until 86% at 10^{-3}M. The variation of the inhibition efficiency (E_w%) versus the concentration for both molecule is illustrated in Figure 3. The inspection of these data reveals that the protection efficiency increases with increasing the concentration of the inhibitor and reaches a maximum (**86%**) at 10^{-3}M.

Table 1 : Corrosion rate and inhibition efficiency in absence and presence of inhibitor in 1M HCl.

Concentrations	w_{corr} (mg/cm^2 .h)	Θ	E (%)
HCl (1M)	0.826	--	--
10^{-6}M	0.412	0.50	50
10^{-5}M	0.306	0.63	63
10^{-4}M	0.234	0.72	72
10^{-3}M	0.119	0.86	**86**

3.2. Adsorption isotherm and thermodynamic parameter:

The relationship between the surface covered θ and the concentration C is a practical method to read out nature of adsorption isotherm by fitting graphics to various isotherms [16].As the Figure 4 shows the adsorption isotherm plots for each inhibitor, Langmuir's isotherm seems to be the best-fitting model for the experiment results, it assumes that the solid surface contains a fixed number of adsorption sites and each site holds one adsorbed species[17]. The following equation is applied:

$$\frac{C}{\theta} = \frac{1}{K} + C \quad \textbf{(9)}$$

Where C_{inh} is the concentration of inhibitor, K_{ads} is the adsorptive equilibrium constant of the adsoption process which is related to the the standard Gibbs energy of adsorption, ΔG_{ads} to the following equation [18]:

$$\Delta G_{ads} = -RT.ln(55,5.K) \qquad \textbf{(10)}$$

where R is the universal gas constant, T is the thermodynamic temperature and the value of 55.5 is the concentration of water in the solution in mol/L.
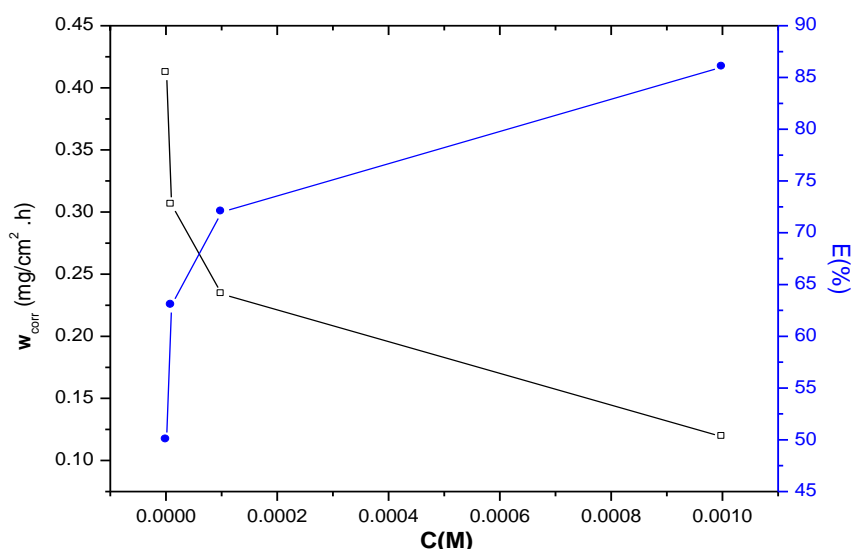

Figure 3: Variation of the inhibition efficiency with the inhibitor 1,4-diallyl-6-methylquinoxaline-2,3(1H,4H)-dione (**2**) concentration in 1M HCl.

The results are listed in Table 2, a very good fit is observed with the regression coefficients up to 0.99, which suggests that the experimental data are well described by Langmuir isotherm. From the intercepts of the straight lines C_{inh}/h-axis, the K_{ads}values were calculated and given in Table 2. The calculated ΔG_{ads} values, using Eq. (10), were also given in Table 2. The large negative values of ΔG_{ads} ensure the spontaneity of the adsorption process and the stability of the adsorbed layer on the mild steel surface as well as a strong interaction between inhibitors and the metal surface [19]. Figure 4 Langmuir isotherm adsorption model of each inhibitors on steel surface in HCl 1M solution.

Table 3: Thermodynamics parameters adsorption of inhibitor 1,4-diallyl-6-methylquinoxaline-2,3(1H,4H)-dione (**2**) on the steel mild in HCl 1M media.

Inhibitor	Slope	R^2	K_{ads} (M^{-1})	$\Delta G°_{ads}$ (kJ mol^{-1})
(**2**)	1.16224	0.999	$1.09 \ 10^5$	-34.03

Generally, the energy values of *-20 kJ.mol^-1* or less negative are associated with an electrostatic interaction between charged molecules and charged metal surface, physisorption; those of *-40 kJ.mol^-1* or more negative involve charge sharing or transfer from the inhibitor molecules to the metal surface to form a coordinate covalent bond, chemisorption[20], in our case, the values of ΔG_{ads}rang from *-30 kJ.mol^-1* to *-40 kJ.mol^-1* (table 3) it is suggested that adsorption of our molecules involves two type of interaction, chemisorption and physisorption.

3.3. Electrochemical Measurements
3.3.1. Tafel Polarization Study

The representative potentiodynamic polarization curves of the mild steel electrode, which were obtained in 1M HCl solution in the absence and presence of various concentrations of 1,4-diallyl-6-methylquinoxaline-2,3(1H,4H)-dione (**2**) are given in Figure 5. In order to obtain information about the kinetics of the corrosion, some electrochemical parameters, i.e., corrosion potential (E_{corr}), corrosion current density (I_{corr}) and cathodic (βc) Tafel slopes and inhibition efficiency (Ep %) values were calculated from the corresponding polarization curves and the obtained data are given in Table 4.
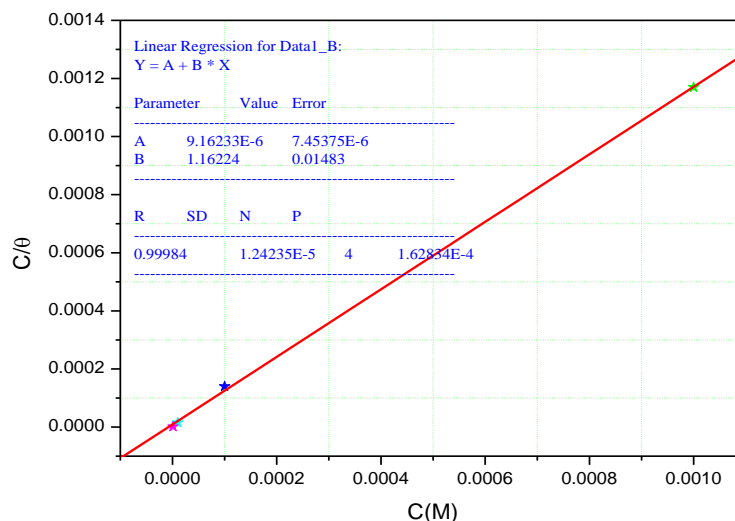
Figure 4: C⁄θ versus C plots for mild steel in 1 M HCl at 308K at the presence of θis mean values of surface coverage from potentiodynamic polarization measurements).
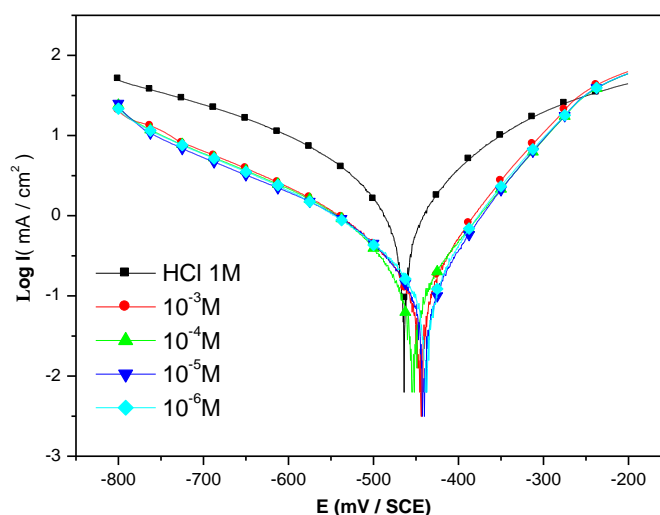

Figure 5: Polarization curves of steel mild in1.0 M HCl with and different concentrations of 1,4-diallyl-6-methylquinoxaline-2,3(1H,4H)-dione (**2**) at 308K.

It can be noticed that the curves shift towards lower current density region in the presence of the inhibitor compared to the blank acid medium. This suggests that the studiedcompound1,4-diallyl-6-methylquinoxaline-2,3(1H,4H)-dione (**2**) reduce the corrosion current and therefore reduce the corrosion rate. The suppression effect becomes more pronounced with the increase of the concentration of inhibitor 1,4-diallyl-6-methylquinoxaline-2,3(1H,4H)-dione (**2**).The polarization curves also exhibit shifts in potential towards more cathodic regions relative to the acid blank. We can classify an inhibitor as cathodic or anodic type if the displacement in corrosion potential is more than 85 mV with respect to corrosion potential of the blank [21, 22].In the presence of inhibitor1,4-diallyl-6-methylquinoxaline-2,3(1H,4H)-dione (**2**), the corrosion potential of mild steel shifted to the negative side only 18 mV (vs. SCE) for 1,4-diallyl-6-methylquinoxaline-2,3(1H,4H)-dione (**2**).This can be interpreted that tested inhibitor acts as a mixed type inhibitor and shows more pronounced influence in the cathodic polarization plots compared to that in the anodic plots. The data in Table 4 reveals that when the concentration of 1,4-diallyl-6-methylquinoxaline-2,3(1H,4H)-dione (**2**).increased, the inhibition efficiency increases and the corrosion current density decreases sharply. This may be due to the adsorption layer of the inhibitor on the metal surface

Table 4: Polarization parameter for the corrosion of steel in HCl 1M acid with and without 1,4-diallyl-6-methylquinoxaline-2,3(1H,4H)-dione (**2**) at 308K.

Inhibitor	Concentration (M)	-E_{corr}	I_{corr} ($\mu A/cm^2$)	-βc	E (%)
1M HCl	-	465	1386	184	--
	10^{-6}	449	591	185	59
	10^{-5}	447	432	175	70
(2)	10^{-4}	451	250	191	84
	10^{-3}	448	137	183	**89**

3.3.2. Electrochemical impedance spectroscopy (EIS)

The corrosion behavior of mild steel in 1M HCl solution with and without inhibitor 1,4-diallyl-6-methylquinoxaline-2,3(1H,4H)-dione (**2**) is also investigated by the electrochemical impedance spectroscopy (EIS) at 308 K after 30 min of immersion, The Figure 6 and Figure 7 shows the Nyquist and Bode diagrams obtained at open-circuit potential, when adding inhibitor 1,4-diallyl-6-methylquinoxaline-2,3(1H,4H)-dione (**2**) to the aggressive medium it always lead to an increase in the large of the semi circles curve of impedance diagrams by increasing the concentration of each inhibitor likewise the inhibition efficiencies.
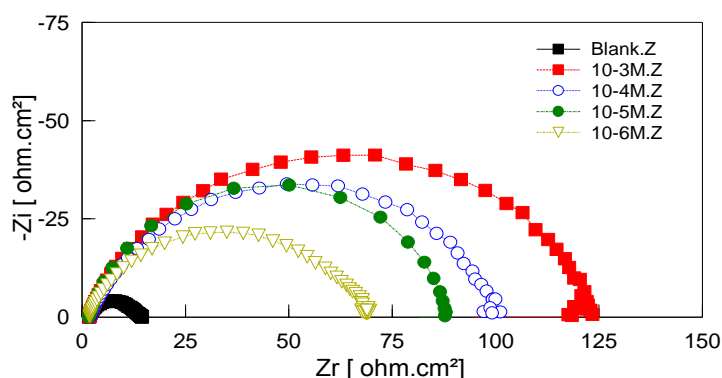

Figure 6 : Impedance diagrams for the corrosion of steel in HCl 1M with and without inhibitor at 308K at E_{corr}.
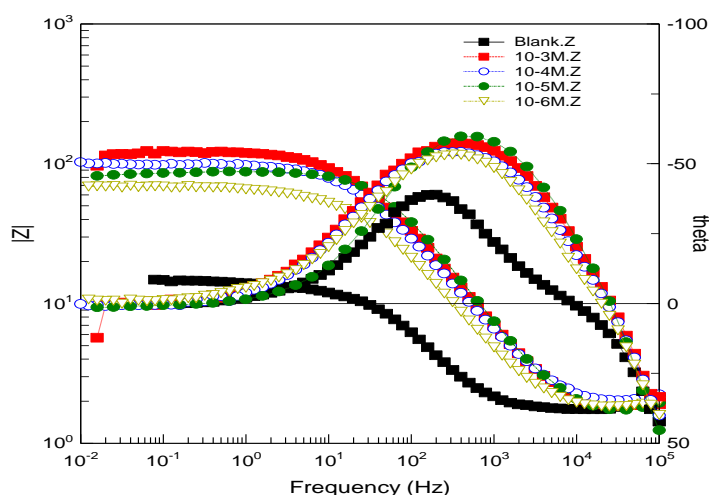

Figure 7 : Electrochemical impedance Bode-Phase plots of mild steel in 1 M HCl with different concentration of 1,4-diallyl-6-methylquinoxaline-2,3(1H,4H)-dione (**2**).at OCP and 308K.

In order to determine the impedance parameters from the experimental results, the data were fitted to the electrical equivalent circuit using the Zview software. Figure 8 represents the electrical equivalent circuit in the

absence and presence of inhibitor 1,4-diallyl-6-methylquinoxaline-2,3(1H,4H)-dione (**2**). Excellent fit results in Figure 9 were obtained using this circuit. In the equivalent circuit, Rs is the uncompensated solution resistance, R_{ct} refers to the charge-transfer resistance and CPE is the constant phase element (CPE). The calculated impedance parameters derived from the complex plane plots are given in Table 5. In this case, due to the depression resulted by surface heterogeneity at a micro- or nano-level, such as the surface roughness/porosity, adsorption or diffusion, an acceptable fit could be obtained only if a CPE is used instead of capacitance in the equivalent circuit models [23-24].

Table 5 : EIS parameter for the corrosion of mild steel in HCl 1M acid with and without inhibitor at 308K.

| Concentration (M) / Prameters	1M HCl	10^{-6}	10^{-5}	10^{-4}	10^{-3}
Real Center	9.25	35.34	44.25	51.02	61.06
Imag. Center	1.62	15.63	8.58	18.02	16.95
Diameter	15.13	74.54	86.04	104.19	121.67
n	0.81	0.78	0.84	0.81	0.79
Low Intercept $R_s(\Omega.cm^2)$	1.86	1.50	2.10	2.13	2.63
High Intercept $R_t(\Omega.cm^2)$	16.64	69.17	86.41	99.90	119.49
Depression Angle	12.42	24.80	11.51	20.23	16.18
ω_{max}(rad s^{-1})	929.60	154.01	306.93	149.09	134.08
Estimated $R_t(\Omega.cm^2)$	14.78	67.67	84.30	97.76	116.85
Estimated $C_{dl}(F.cm^{-2})$	7.11 E-5	6.7098E-5	5.7867E-5	4.4372E-5	4.13E-5
E (%)	--	77	82	84	**88**
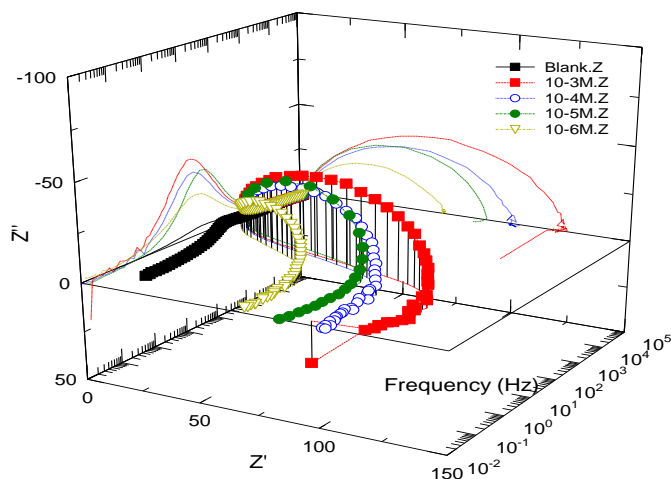
Figure 8 : EIS Nyquist and Bode diagrams 3D for mild steel/1 M HCl + Inhibitor interface: (**------**) experimental; (**------**) fitted data.

As evident from Table 5, the values of charge-transfer resistance have increased with increasing the inhibitor concentration. This may be attributed to the decrease in local dielectric constant and/or to the increase in the thickness of the electrical double layer [25-26]. These results suggest that the 1,4-diallyl-6-methylquinoxaline-2,3(1H,4H)-dione (**2**) act just via adsorption at the metal/solution interface.

The dissolution mechanism could be predicted by the values of phase shift (n) as an indicator. It is clear that, no significant change in the value of n is observed after addition of various concentrations 1,4-diallyl-6-

methylquinoxaline-2,3(1H,4H)-dione (**2**) (Table 5). The almost invariable values of n indicates that the charge transfer process controls the dissolution mechanism in both the absence and presence of various concentrations of 1,4-diallyl-6-methylquinoxaline-2,3(1H,4H)-dione (**2**) [27].
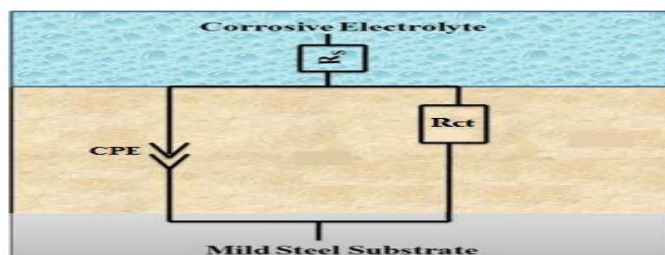

Figure 9 : Equivalent circuit used to model metal/solution interface of mild steel in 1 M HCl in the absence and presence of inhibitor (for equivalent circuit diagram, Rs: uncompensated solution resistance, R_{ct}: charge-transfer resistance and CPE: constant phase element.
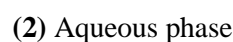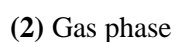
3.4. Quantum chemical calculations

The FMOs (HOMO and LUMO) are very important for describing chemical reactivity. The HOMO containing electrons, represents the ability (E_{HOMO}) to donate an electron, whereas, LUMO haven't not electrons, as an electron acceptor represents the ability (E_{LUMO}) to obtain an electron. The energy gap between HOMO and LUMO determines the kinetic stability, chemical reactivity, optical polarizability and chemical hardness–softness of a compound [28]. Firstly, in this paper, we calculated the HOMO and LUMO orbital energies by using B3LYP method with 6-31G(d,p). All other calculations were performed using the results with some assumptions. The higher values of E_{HOMO} indicate an increase for the electron donor and this means a better inhibitory activity with increasing adsorption of the inhibitor on a metal surface, where as E_{LUMO} indicates the ability to accept electron of the molecule. The adsorption ability of the inhibitor to the metal surface increases with increasing of E_{HOMO} and decreasing of E_{LUMO}. The HOMO and LUMO orbital energies and image of 1,4-diallyl-6-methylquinoxaline-2,3(1H,4H)-dione (**2**) were performed and were shown in Table 6 and Figure 10. High ionization (I= 6.741 eV, I= 6.940 eV in gas and aqueous phases respectively) indicates high stability [29], the number of electrons transferred (ΔN) was also calculated and tabulated in Table 6. The $\Delta N < 3.6$ indicates the tendency of a molecule to donate electrons to the metal surface [30-31].

Table 6 : Quantum chemical descriptors of the studied inhibitors at B3LYP/6-31 G** in gas, G and aqueous, A phases and the inhibition efficiencies as given in [32, 33].

Prameters	Phase	
	Gas	**Aqueous**
Total Energy *TE* **(eV)**	-16537.4	-16537.9
E_{HOMO} **(eV)**	-6.741	-6.940
E_{LUMO} **(eV)**	0.007	0.110
Gap *ΔE* **(eV)**	6.748	7.050
Dipole moment *μ* **(Debye)**	5.761	7.773
Ionisation potential *I* (eV)	6.741	6.940
Electron affinity *A*	-0.007	-0.110
Electronegativity *χ*	3.367	3.415
Hardness *η*	3.374	3.525
Electrophilicity index *ω*	1.680	1.654
Softness *σ*	0.296	0.283
Fractions of electron transferred *ΔN*	0.538	0.508

The final optimized geometries of (**2**) in gas and aqueous, selected valence bond angle and dihedral angles and bond lengths are given in Figure 10.

(**2**) Gas phase   (**2**) Aqueous phase

Figure 10. Optimized molecular structures, selected dihedral angles (red), valence bond angle (blue) and bond lengths (black) of the studied inhibitors calculated in gas and aqueous phases at B3LYP/6-31G(d,p) level of (**2**)

Table 8 : The HOMO and the LUMO electrons density distributions of the studied inhibitors computed at B3LYP/6-31G (d,p) level in gas and aqueous phases.

	(**2**) Gas phase	(**2**) Aqueous phase
HOMO		
LUMO		

After the analysis of the theoretical results obtained, we can say that the molecule (**2**) have a non-planar structure. The inhibition efficiency afforded by the quinoxaline derivative (**2**) may be attributed to the presence of electron rich O.

3.5. Scanning electron microscopy

The surface analysis of mild steel immersed in HCl and inhibitor was done. It is clear from the Figure 11 (a, b, c) showing the SEM micrographs of polished mild steel, mild steel immersed in HCl and mild steel immersed in inhibitor solution that (b) has rough surface with cavities and pores whereas (c) has lesser cavities and less rough surface. Thus, it can be thought of an evidence of adsorption of inhibitor on the surface of mild steel [34].
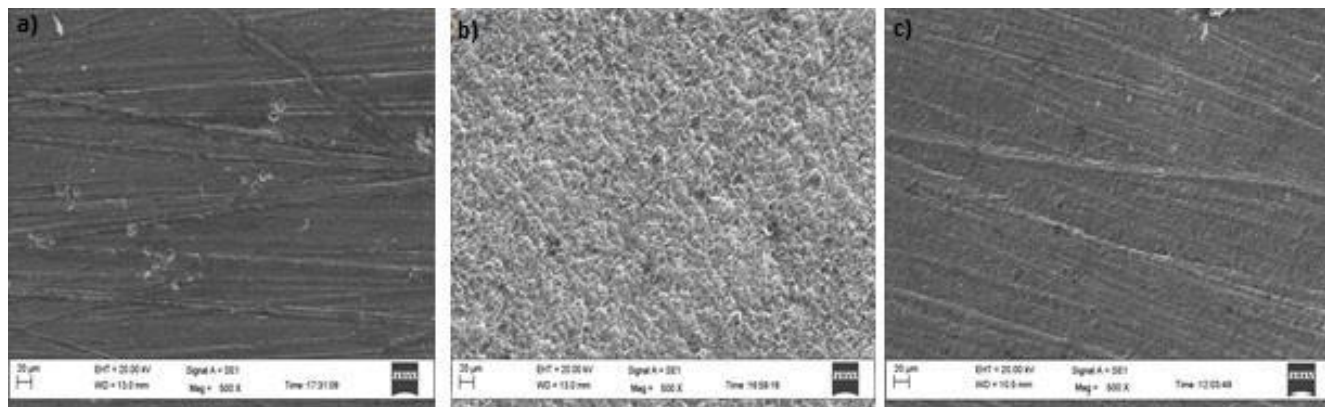
Figure 11: SEM images for a) Polished mild steel, b) mild steel in HCl, c) mild steel in Inhibitor.

The morphology in figure (11c) shows a rough surface, characteristic of uniform corrosion of mild steel in acidic medium, as previously reported, that corrosion does not occur in presence of inhibitor and hence corrosion was inhibited strongly when the inhibitor was present in the hydrochloric, and the surface layer is very rough. In contrast, in the presence of 10^{-3}M of 1,4-diallyl-6-methylquinoxaline-2,3(1H,4H)-dione (**2**), there is much less damage on the mild steel surface, which further confirms the inhibition action. Also, there is an adsorbed film on mild steel surface (Figure (11c)). In accordance, it might be concluded that the adsorption film can efficiently inhibits the corrosion of mild steel.

Conclusion

The corrosion inhibition of mild steel in 1.0 M HCl solutions by 1,4-diallyl-6-methylquinoxaline-2,3(1H,4H)-dione (**2**) was studied using common electrochemical techniques and quantum chemical calculations by DFT. According to experimental and theoretical findings, it could be concluded that:

- ✓ 1,4-diallyl-6-methylquinoxaline-2,3(1H,4H)-dione (**2**) is a good corrosion inhibitor for the mild steel protection in both acid solutions. The inhibitory efficiency of this compound depends on its concentration in both acid solution.
- ✓ EIS plots indicated that R_{ct} values increase and C_{dl} values decrease with increasing inhibitor concentration.
- ✓ Polarization curves indicated that 1,4-diallyl-6-methylquinoxaline-2,3(1H,4H)-dione (**2**) act as mixt type inhibitor.
- ✓ The adsorption of 1,4-diallyl-6-methylquinoxaline-2,3(1H,4H)-dione (**2**) on the steel surface follow Langmuir adsorption isotherm. The thermodynamic parameters suggest that this inhibitor is strongly adsorbed on the mild steel surface.
- ✓ The quantum chemical parameters (such as E_{HOMO}, E_{LUMO}, and dipolar moment) are obtained and discussed in view of experimental results.
- ✓ Both experimental and quantum chemical results showed that the inhibition efficiency of 1,4-diallyl-6-methylquinoxaline-2,3(1H,4H)-dione (**2**) is affected by the heteroatoms and π-system presented in our compound.

References
1. Deepika Y., Sachin K., Shewta S., *Int. J. Curr. Pharm. Rev. Res.*, 3 (3) (2011)71-73.
2. Chadli R., Elazouzi M., Khelladi I., Elhourri A.M.,Elmsellem H.,Aouniti A., KajimaMulengi J., Hammouti

B., *Portugaliae Electrochimica Acta.* 35(2017) 65-80.

3. Benbouya K., Zerga B., Sfaira M., Taleb M., Ebn Touhami M., Hammouti B., Benzeid H., Essassi E.M., *Int. J. Electrochem. Sci*., 7 (2012) 6313 – 6330.

4. Olasunkanmia L.O., Kabandaa M.M., Ebenso E.E., *Physica., E* 76 (2016) 109–126.

5. Kabanda M.M., Ebenso E.E., Int. *J. Electrochem. Sci*., 7 (2012) 8713-8733.

6. Dong Wook Chang, Seo Jin Ko, Jin Young Kim, Liming Dai, Jong-Beom Baek*, Synth. Met*. 162 (2012) 1169–1176.

7. Carta A., Paglietti G., Nikookar M.E.R., Sanna P., Sechi L., Zanetti S., *Eur. J. Med. Chem*., 37(2002) 355-366.

8. El-Sabbagh O. I, El-Sadek M.E, Lashine S.M, Yassin S.H, El-Nabtity S.M., *Med. Chem. Res*., 18(2009)782–797.

9. Gupta D., Ghosh N.N., Chandra R., *Bioorg.Med.Chem Lett*. 15 (2005)1019–1022.

10. Sarges R., Howard H. R., Browne R. G., Lebel L. A., Seymour P.A., Koe B. K., *J. Med. Chem*.,33 (1990)2240–2246.

11. Elmsellem H., Basbas N., Chetouani A., Aouniti A., Radi S., Messali M., Hammouti B., *Portugaliae. Electrochimica. Acta*. 2 (2014) 77.

12. Koopmans T. C., *Physica. Amsterdam.,* 1 (1934) 104

13. Sastri V.S., Perumareddi J.R., *Corrosion*., 53 (1997) 617.

14. Elmsellem H., Nacer H., Halaimia F., Aouniti A., Lakehal I., Chetouani A., Al-Deyab S. S., Warad I., Touzani R., Hammouti B., *Int. J. Electrochem. Sci*., 9(2014)5328.

15. Udhayakala P., Rajendiran T. V., Gunasekaran S., *J.C.B.P.S*., 2(3) (2012)1151–1165.

16. Singh A., Ebenso E. E., Quraishi M. A., *Int. J. Electrochem. Sci*., 7 (2012) 4766.

17.Tribak Z., KandriRodi Y., Elmsellem H., Abdel-Rahman I., Haoudi A., Skalli M. K., Kadmi Y., Hammouti B., Ali Shariati M., Essassi E. M., *J. Mater. Environ. Sci*., 8 (2017) 1116 -1127.

18. Ahamad I., Prasad R., Quraishi M. A., *J. Solid. State.Electrochem*.,14 (2010) 2095.

19. El Ouadi Y., Manssouri M., Bouyanzer A., Majidi L., Bendaif H., Elmsellem H., Shariati M.A., Melhaoui A., Hammouti B., *Microbial Pathogenesis* .107 (2017) 1-6.

20. Fouda S., Mahmoud W. M., Abdul Mageed H. A., *J. Bio.Tribo.Corros*., 2 (2016) 1.

21. Benabdellah M., Aouniti A., Dafali A., Hammouti B., Benkaddour M., Yahyi A., Ettouhami A., *Appl. Surf. Sci*. 252 (2006) 8341–8347.

22. Elmsellem H., Aouniti A., Youssoufi M.H., Bendaha H., Ben hadda T., Chetouani A., Warad I., Hammouti B., *Phys. Chem. News*. 70 (2013) 84.

23. Bendaha H., Elmsellem H., Aouniti A., Mimouni M., Chetouani A., Hammouti B., *Physicochemical Mechanics of Materials.,* 1 (2016) 111-118.

24. Hjouji M. Y., Djedid M., Elmsellem H., Kandri Rodi Y., Ouzidan Y., OuazzaniChahdi F., Sebbar N. K., Essassi E. M., Abdel-Rahman I., Hammouti B., *J. Mater. Environ. Sci*., 7(4)(2016)1425-1435.

25. Sikine M., Kandri Rodi Y., Elmsellem H., Krim O., Steli H., Ouzidan Y., Kandri Rodi A., OuazzaniChahdi F., Sebbar N. K., Essassi E. M., *J. Mater. Environ. Sci*., 7 (4) (2016) 1386-1395.

26. EL Aoufir Y., Lgaz H., Bourazmi H., Kerroum Y., Ramli Y., Guenbour A., Salghi R., El-Hajjaji F., Hammouti B., Oudda H., *J. Mater. Environ. Sci*. 7 (12) (2016) 4330-4347

27. Elmsellem H., Basbas N., Chetouani A., Aouniti A., Radi S., Messali M., Hammouti B., *Portugaliae. Electrochimica. Acta*., 2 (2014) 77.

28. Govindarajan M., Karabacak M., *Spectrochim. Acta Part A Mol Biomol Spectrosc*., 85 (2012) 251.

29. Fouda A.S., Shalabi S.K., Elewady G.Y., Merayyed H.F., *Int. J. Electrochem. Sci*. 9 (2014) 7038.

30. Lukovits I., Kalman E., Zucchi F., *Corrosion*., 57 (2001) 3.

31. Obot I.B., Obi-Egbedi N.O., Umoren S.A., *Corros. Sci*., 51 (2009) 1868.

32. Becke A.D., *J. Chem. Phys*. 98 (1993)1372.

33. Kumar S., Ladha D. G., Jha P. C., and Shah N. K., International Journal of Corrosion Volume (2013), ID 819643, 10 http://dx.doi.org/10.1155/2013/819643.

34. Obot I.B., Obi-Egbedi N.O., *Corros. Sci*. 52 (2010) 198.

(2017); http://www.jmaterenvironsci.com/